Journal of Materials Chemistry

Cite this: J. Mater. Chem., 2012, 22, 4637

www.rsc.org/materials

COMMUNICATION

# Zeolite nanosheet of a single-pore thickness generated by a zeolite-structure-directing surfactant†

Jinhwan Jung, Changbum Jo, Kanghee Cho and Ryong Ryoo*

*Received 12th December 2011, Accepted 27th January 2012*
**DOI: 10.1039/c2jm16539b**



**Zeolite MFI nanosheets have been hydrothermally synthesized using a surfactant with the formula $[C_{18}H_{37}–N^+(CH_3)_2–C_6H_{12}–N^+(CH_3)_2–C_6H_{12}–N^+(CH_3)_2–C_{18}H_{37}][Br^-]_3$ as the zeolite structure-directing agent. These nanosheets correspond to a slice of MFI zeolite crystal of 1.5 nm thickness in the *b*-direction. Each nanosheet is composed of a monolayer of micropores, which is thinner than a single crystal unit-cell dimension (2.0 nm). Such a single-pore zeolite nanosheet still exhibits high thermal stability, steam stability, acid strength and shape-selective catalytic activity, comparable to the bulk crystal.**

In a crystal, the constituent atoms or molecules are arranged in a regularly ordered manner, repeating the arrangement pattern into three-dimensional space. The smallest repeating unit in a crystal is the unit cell, which is commonly used to define a crystal structure. Over the past few decades, many studies have focused on size reduction of solid crystals to nanoscale architectures such as nanoparticles, nanorods and nanosheets. Nanosizing often causes a remarkable change in physical and chemical properties as compared to bulk properties.[1] Moreover, because a large portion of constituent atoms is located on the external surfaces, nanoscale architectures can provide an opportunity for obtaining a fundamental insight into the surface properties like adsorption and catalysis.[2]

Zeolites are a family of crystalline microporous aluminosilicate minerals with various pore topologies (about 200 structure types) and pore diameters (typically ranging from 0.3 to 1.5 nm).[3] Many zeolites can support (or host) catalytically active transition metal nanoparticles inside uniform micropores. Zeolites have high gas adsorption capacity due to the high specific surface area of the microporous structure. They have excellent thermal stability, hydrothermal stability and mechanical strength.[3,4] In most zeolites, trivalent Al atoms are tetrahedrally coordinated by oxygen in the crystalline silicate framework. This causes a charge mismatch, which is compensated by the extra-framework $Na^+$ ions. The sodium ions can be exchanged with other cations like $K^+$ or $H^+$. In some zeolites, the $H^+$-ionic form can exhibit Lewis acidity and also Brønsted acidity, which is comparable to the case of sulfuric acid.[5] Due to these properties, zeolites are widely used as heterogeneous catalysts in the chemical industry, particularly in oil refineries and in petrochemical processing.[4,5]

In many catalytic applications, however, the long diffusion path length inside bulkily crystalline zeolite can cause serious diffusion limitations. Lercher and co-workers reported that the mass transfer for zeolites of less than 100 nm is not hindered by diffusion.[6] Thus, the diffusion limitations can be overcome by decreasing the crystal thickness.[6] Many studies in recent years have focused on the preparation of zeolites in the form of nanocrystals, nanosheets, nanosponges, and other hierarchically porous architectures.[7] Most notably, Ryoo and co-workers synthesized zeolite MFI nanosheets of 2.5 nm thickness using a diammonium surfactant as a structure-directing agent (SDA) for the zeolite instead of the commonly used tetrapropylammonium.[8] In the bottom-up synthesis approach, the surfactant molecules were organized into a lamellar mesostructure while the ammonium groups in each surfactant acted as the zeolite SDA. In this manner, the surfactant molecule had a dual structure-directing ability in two different length scales: pore generation in the microscale and nanosheet generation in the mesoscale. This was the first report convincing that a zeolite micropore could really be synthesized by the porogenic activity of a functional group of a molecule, rather than by the entire molecule, as in conventional zeolite synthesis. The resultant 2.5 nm nanosheet consisted of three pentasil layers. Later, Na *et al.* showed that the dual SDA strategy could be extended to the synthesis of mesoporous materials with zeolitic walls.[9] Thus far, the 2.5 nm sample was the thinnest possible MFI zeolite that could be crystallized through synthetic approaches. The thickness was close to a single unit-cell dimension (2.0 nm) along the *b*-axis of the MFI crystal structure.[8]

On the contrary to the aforementioned synthetic approach, the Corma group did a top-down analytical approach to obtain zeolite nanosheets. They did layer-by-layer separation of a precursor to MWW zeolite before calcination, obtaining delaminated zeolite nanosheets corresponding to a single unit-cell dimension.[10] In the case of FER, delamination yielded zeolite nanosheets that were even thinner than a single unit cell.[11] It was believed that this type of post-synthetic fragmentation, *i.e.*, a top-down approach, was applicable only for zeolites that could exist as a layered material in a precursor state before final conversion to a 3-dimensional zeolite crystal *via* calcination. Recently, the Cejka group demonstrated that the

*Department of Chemistry, and Graduate School of Nanoscience and Technology (WCU), KAIST, Daejeon, 305-701, Korea. E-mail: rryoo@kaist.ac.kr; Fax: +82-42-350-8130; Tel: +82-42-350-2870*

† Electronic supplementary information (ESI) available: Schematic diagram of various surfactants, electron diffraction pattern, $N_2$ isotherms, thermal/steam thermal stability test, and ammonia TPD. See DOI: 10.1039/c2jm16539b

delaminating strategy could be extended to a 3-dimensional zeolite possessing a layer of 4-membered-ring (4MR) portion within the crystal structure. They obtained sub-unit-cell nanolayers of FER zeolite by breaking the 4MR portion of the UTL zeolite.[12]

In the present work, we were interested in the lower limit for zeolite thickness that could be achieved by the bottom-up approach using dual structure-directing surfactants. After trying many surfactants, we discovered that a Gemini-type triammonium surfactant, $[C_{18}H_{37}$–$N^+(CH_3)_2$–$C_6H_{12}$–$N^+(CH_3)_2$–$C_6H_{12}$–$N^+(CH_3)_2$–$C_{18}H_{37}][Br^-]_3$, could generate zeolite nanosheets, which corresponded to an extremely thin slice of MFI zeolite crystal of 1.5 nm thickness in the *b*-direction. Thus, the nanosheets were even thinner than a single crystal unit-cell dimension (2.0 nm) in the *b*-direction (see below for structure analysis). This zeolite sample is denoted by SPZ, which stands for 'single-pore zeolite'. The SPZ was hydrothermally synthesized under basic conditions. In brief (see ESI† for the synthesis details), GS-3N surfactant, sodium aluminate (Sigma-Aldrich, 53 wt% $Al_2O_3$, 42.5% $Na_2O$) and tetraethylorthosilicate (TCI, 98%) were well mixed with an aqueous solution containing sodium hydroxide. The resultant gel had a molar composition of 1.0 GS-3N : 30.0 $SiO_2$ : 0.15 $Al_2O_3$ : 6.6 $Na_2O$ : 1070 $H_2O$. The mixture was heated for 8 d in an oven at 413 K with tumbling. The SPZ product was collected by filtration. After drying at 403 K, the product was calcined in air under static conditions at 853 K, in order to remove organic surfactants. After calcination, organic surfactants were completely removed from the zeolite framework, which was confirmed by TGA analysis. The structure was characterized by transmission electron microscopy (TEM) in combination with the X-ray powder diffraction (XRD) pattern.

Structure determination was first approached by comparing the XRD pattern of SPZ with the 'standard' database provided by the International Center for Diffraction Data using MDI Jade 5.0. As shown in Fig. 1(A), the XRD pattern of the SPZ sample was well matched to (*h*0*l*) reflections of MFI zeolite. The absence of the reflections along the *b*-direction indicates that the zeolite should be extremely thin in the *b*-direction. To determine the structure more clearly, a TEM investigation was performed as shown in Fig. 1(B) and 2(A)–(C). The TEM image in Fig. 1(B) could be explained with 1.5 nm thick zeolite nanosheets separated by 1.7 nm organic layers. High-resolution TEM images and the corresponding electron diffraction patterns were taken along the 3 perpendicular zone axes.

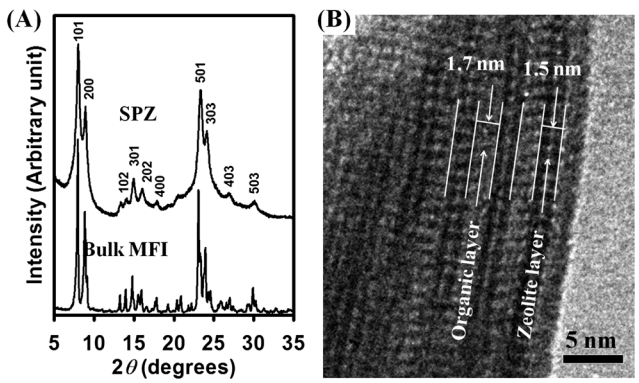


**Fig. 1** XRD pattern (A) and TEM image (B) of zeolite nanosheets as synthesized using $[C_{18}H_{37}$–$N^+(CH_3)_2$–$C_6H_{12}$–$N^+(CH_3)_2$–$C_6H_{12}$–$N^+(CH_3)_2$–$C_{18}H_{37}][Br^-]_3$ surfactant as a zeolite-structure-directing agent.

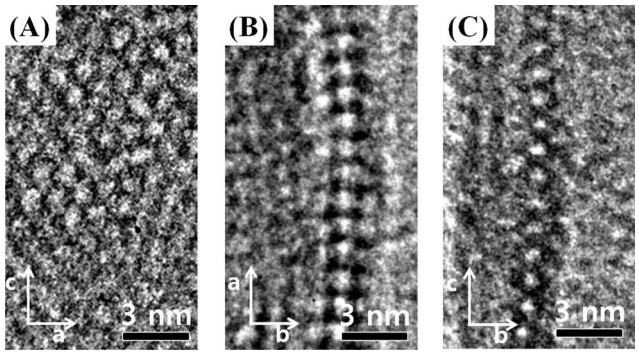


**Fig. 2** TEM images of a 1.5 nm thick zeolite nanosheet projected down the [010] (A), [001] (B) and [100] (C) zone axes.

As the result in Fig. 2(A)–(C) and S1† shows, each zeolite layer is well matched to an MFI nanosheet, which is wide in the *ac* plane and 1.5 nm thick in the *b*-direction. This nanosheet corresponds to a single layer of micropores along the *b*-axis in the MFI zeolite structure, including the upper and lower frameworks, as provided by the International Zeolite Association. The 1.5 nm thickness is a mean value between the maximum thickness of 1.7 nm and the minimum thickness of 1.3 nm (Fig. S2†). The thickness is only 3/4 of the *b* lattice parameter ($b = 1.97$ nm). Strictly speaking, it is not yet possible to define uniquely the framework topology as MFI because the thickness is less than the MFI unit-cell parameter. For instance, the zeolite nanosheet may be of another structure type whose unit cell is equal to the *b*/2 portion of the MFI unit cell. Nevertheless, SPZ may not be assigned to an MEL-type zeolite. MFI has zigzag channels within the *ac* plane, but MEL has only straight channels. Due to this difference, an MEL-type zeolite cannot exhibit the (102) reflection assigned in Fig. 1(A). For convenience, we describe SPZ as the first example of an MFI zeolite thinner than a single-unit-cell dimension that could be obtained *via* the bottom-up synthesis approach thus far. To the best of our knowledge, SPZ is the thinnest sample among all zeolites with micropores synthesized by the bottom-up approach.

The zeolite-structure-directing function of the surfactant head group was further investigated by substituting the triammonium moiety in the GS-3N surfactant with $–[N^+(CH_3)_2–C_6H_{12}–]_4$ and $–[N^+(CH_3)_2–C_6H_{12}–]_5$ (Fig. S3†). Hydrothermal synthesis of zeolite was performed using the resultant surfactants (GS-4N and GS-5N, respectively). Both GS-4N and GS-5N generated MFI zeolite nanosheets, but the nanosheet thickness changed according to the number of ammoniums (Fig. S4†). The zeolite nanosheet from GS-4N was composed of two layers of micropores, which was 2.5 nm thick along the *b* axis. The number of micropore layers further increased to 3 in the case of GS-5N, so that the thickness became 3.5 nm. It is noteworthy that the number of micropore layers increased in proportion to $n - 2$ in this surfactant series, where $n$ is the number of ammoniums in a surfactant head. This result indicates that, among the $n$ ammonium groups, the two *tailed* ones [*i.e.*, $–N^+(CH_3)_2–$ bonded directly to $C_{18}H_{37}$–tail] did not contribute to the nanosheet thickness. The tailed ammoniums seemed to be located outside the zeolite nanosheet while the *inner* ammonium groups participated in the formation of zeolite pores inside the nanosheet. We tested Gemini-type surfactants containing only the *tailed* ammoniums such as $[C_{18}H_{37}$–$N^+(CH_3)_2$–$C_{18}H_{37}][Br^-]$ and $[C_{18}H_{37}$–$N^+(CH_3)_2$–$C_6H_{12}$–$N^+(CH_3)_2$–$C_{18}H_{37}][Br^-]_2$. However, these surfactants were unable to generate

 

zeolite frameworks at all. It thus seemed that the *tailed* ammonium groups were difficult to function as a zeolite SDA by themselves. We suggest that the *tailed* ammonium groups would be necessary as a linker between a long alkyl tail and *inner* ammoniums in order to provide the *inner* ammoniums sufficiently high molecular degrees of freedom for the zeolite-structure-directing function.

A SPZ sample could be obtained in the ordered multilamellar arrangement of nanosheets shown in Fig. 1(B), or in a manner somewhat disordered (Fig. S5†). The arrangements depended on the details of synthesis conditions, similar to the previous case in the synthesis of 2.5 nm MFI nanosheets.[8] The multilamellar SPZ exhibited small-angle X-ray reflections at $2\theta = 1.8°$ and 3.6° before calcination. These reflections disappeared upon the removal of the surfactant by calcination, due to the interlayer coalescence. There was a significant loss of the intersheet mesopores, too. In the case of a fully disordered nanosheet assembly, no small-angle reflections were detected at all. The nanosheets were rigidly supported by each other, so that the intersheet mesopores were well retained even after calcination (BET area = 840 $m^2 g^{-1}$, total pore volume = 0.96 mL $g^{-1}$). The mesopore diameters were analyzed with the adsorption branch of the nitrogen adsorption isotherm (at 77 K) according to the Barrett–Joyner–Halenda (BJH) algorithm. The result showed a narrow distribution of mesopore diameters centered at 3.8 nm. These pores could be assigned to the mesopore formation between the nearest neighboring nanosheets. As judged by the narrow distribution, the nanosheets did not seem to be totally disordered but maintained somewhat local coherence.

Steam stability of the nanosheet was investigated in the following manner: a fully disordered SPZ sample with Si/Al = 33 was compared with a bulk MFI zeolite with Si/Al = 40 after calcination at 853 K. These powder samples were heated in fused silica tubing with 100% steam flow at the rate of 0.25 mL $min^{-1}$. Temperature was increased from room temperature to 973 K over 2 h, and maintained there for 2 h. The (501) reflection peak in the XRD profile ($2\theta = 23°$) and the BET surface area were measured after cooling to room temperature. Compared with pristine SPZ, the steamed sample showed a 20% decrease in the XRD intensity and a 14% decrease in the BET area (*i.e.*, from 840 to 720 $m^2 g^{-1}$) (Fig. S6†). On the other hand, bulk zeolite showed no more than a 10% decrease in the XRD intensity or the BET area. Although the nanosheet sample was less stable than the bulk zeolite, considering the high-temperature steaming condition, it is quite remarkable that a zeolite of only 1.5 nm thickness was so stable.

Temperature-programmed desorption (TPD) of $NH_3$ from pristine SPZ showed a peak in the range of 423–523 K and another peak in 573–723 K (Fig. S7†). The higher-temperature TPD peak was used to determine the concentration of strong acid sites in the zeolite framework. The acid concentration determined in this manner was 0.17 mmol $g^{-1}$ before steaming, and changed to 0.082 mmol $g^{-1}$ after steaming (Fig. S7 and Table S1†). This result was similar to the case of bulk MFI, which showed a change from 0.22 to 0.097 mmol $g^{-1}$. This $NH_3$ TPD result was checked by catalytic activity in the methanol-to-hydrocarbon conversion reaction (Table 1). This reaction was chosen as a probe reaction because it was known as a typical reaction that could be catalyzed by strong Brønsted acid sites in zeolite frameworks. The bulk zeolite gave a methanol conversion of 95% while the SPZ sample exhibited 70% conversion. The higher methanol conversion on bulk zeolite can be attributed to the higher concentration of strong acid sites. Anyway, after steaming at 973 K, both catalysts lost the catalytic activities almost completely. By lowering the steaming temperature to 873 K, the bulk zeolite could maintain the catalytic activity of 74% methanol conversion. The catalytic conversion was 35% in the case of the nanosheet sample. Thus, quantitative correlations were difficult to draw between the strong acid-site concentration obtained from $NH_3$ TPD and the catalytic activity data. The $NH_3$ TPD analysis used here was only a crude approximation. Moreover, there could be a significant difference in the catalytic turnover frequency of individual acid sites between the nanosheet and bulk zeolite. The acidity could also be influenced by details of synthesis methods. At any rate, the Brønsted acidity is due to tetrahedral framework Al sites. The $NH_3$ TPD and the catalytic activity data, obtained in the present work, indicate that the structural stability did not go in parallel with the stability of Al sites in the framework. Nonetheless, it is surprising that the single-pore zeolite nanosheets could still exhibit the methanol-to-hydrocarbon reaction activity even after the harsh steaming treatment at 873 K.

Recently, under mild condition with relatively low temperature (773 K), the Weckhuysen group reported that the steam-treated bulk MFI showed high activity in the methanol-to-olefin catalytic reaction compared with pristine bulk MFI.[13] We performed steam treatment of SPZ under the same condition reported by the Weckhuysen group. On the contrary to the previous report, the mild steam treatment of SPZ resulted in a significant loss of catalytic activity (25%). This difference may be explained with mesopore generation by steaming.[14] In the case of bulk zeolites, steaming can generate mesopores. This seemed to cause the catalytic activity to increase, more than compensating the corresponding loss of acid sites. In the case of SPZ, however, the zeolite is already extremely thin, and thus, we believe that there would be no advantage due to mesopore generation.

The SPZ with Si/Al = 33 exhibited high acid catalytic activity for the conversion of bulky molecules (Table 2). These reactions must have occurred at the external surfaces (*i.e.*, outer surfaces of the zeolite nanosheets), whereas the molecules were unable to enter the internal micropores. From this result, it is reasonable that the external surfaces possess strong acid sites that could catalyze these reactions. Compared with nanosheets, the catalytic activity of bulk zeolite was very low because of the relatively low specific area of the external surfaces. In the case of MCM-41-type ordered mesoporous materials, the mesopore walls have large surface areas that are accessible for bulky molecules. Due to their amorphous framework nature, however, the mesoporous materials exhibit low catalytic functions in reactions requiring strong acid sites (Table 2). The strong Brønsted acidity of a crystalline aluminosilicate zeolite is largely due to the Si–O–Al angle strain at ≡Si–O(H)–Al≡ sites. Here, the $H^+$ has the

**Table 1** Catalytic conversion of methanol to hydrocarbons over two zeolite samples[a]

| Sample | Before steaming treatment | Steaming treated at 973 K | Steaming treated at 873 K |
|---|---|---|---|
| SPZ | 70% | 4% | 35% |
| Bulk MFI zeolite | 95% | 12% | 74% |

[a] *Reaction conditions*: WHSV of methanol = 14.1 g $g^{-1}$ $h^{-1}$, catalyst 100 mg, and temperature 623 K. These conversion rates of methanol were measured at 30 min of the reaction.

**Table 2** Catalytic activities of three samples for the conversions of bulky molecules

| Reactions[a] | SPZ | Bulk MFI | Al-MCM-41 |
|---|---|---|---|
| 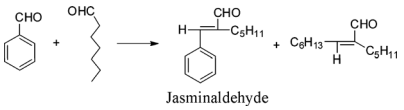 Jasminaldehyde | 85% (70%)[b] | 9% (82%)[b] | <5% |
| 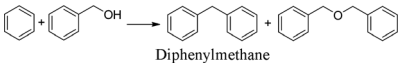 Diphenylmethane | 93% (94%)[c] | 30% (29%)[c] | 12% (81%)[c] |

[a] Catalytic activities were compared on the basis of the same weight of catalysts. [SPZ (Si/Al = 33), bulk MFI (SI/Al = 40)]. [b] Numbers in parentheses indicate jasminaldehyde selectivity. [c] Numbers in parentheses indicate diphenylmethane selectivity.



tendency to dissociate easily. In the noncrystalline aluminosilicate materials, the frameworks are loosely cross-linked and often terminated by SiOH and AlOH (stable H). The frameworks are disorderedly bonded with much less angle strain. This is the reason why these mesoporous materials exhibit low acid catalytic activities.

In conclusion, a zeolite nanosheet composed of only a single layer of micropores was synthesized using a Gemini-type surfactant equipped with a zeolite-structure-directing functional group. This nanosheet corresponded to an extremely thin slice of MFI zeolite crystal, which was wide in the *ac* plane and 1.5 nm thick in the *b*-axis. The crystal thickness was less than a single unit-cell dimension of the MFI structure. Despite the small thickness, the nanosheet was highly stable upon thermal or steam-thermal treatment, retaining strong Al acid sites of the MFI zeolitic nature. The zeolite nanosheet contained strong acid sites on the external surfaces. The zeolite nanosheet was suitable as a catalyst for acid-catalytic reactions involving bulky molecules that could not enter micropores of conventional zeolites. Furthermore, these nanozeolites would be a suitable model to better understand the external surface contribution to catalytic properties.

## Acknowledgements

This work was supported by the National Honor Science Program (20100029665) and World Class University Program (R31-2010-000-10071-0) of the Ministry of Education, Science and Technology in Korea.

## Notes and references

1 R. B. Laughlin, *Phys. Rev. Lett.*, 1983, **50**, 1395; J. Hu, T. W. Odom and C. M. Lieber, *Acc. Chem. Res.*, 1999, **32**, 435; M. Law, J. Goldberger and P. Yang, *Annu. Rev. Mater. Res.*, 2004, **34**, 83; A. K. Geim and K. S. Novoselov, *Nat. Mater.*, 2007, **6**, 183.
2 M. Fernández-García, A. Martínez-Arias, J. C. Hanson and J. A. Rodirguez, *Chem. Rev.*, 2004, **104**, 4063; P. Wen, H. Itoh, W. Tang and Q. Feng, *Langmuir*, 2007, **23**, 11782; N. A. H. Castro, F. Guinea, N. M. R. Peres, K. S. Novoselov and A. K. Geim, *Rev. Mod. Phys.*, 2009, **81**, 109.
3 A. Corma, *Chem. Rev.*, 1997, **97**, 2373; C. S. Cundy and P. A. Cox, *Chem. Rev.*, 2003, **103**, 663.
4 R. A. Sheldon and R. S. Downing, *Appl. Catal., A*, 1999, **189**, 163; R. Rinaldi and F. Schüth, *Energy Environ. Sci.*, 2009, **2**, 610.
5 A. Corma, *J. Catal.*, 2003, **216**, 298.
6 K. Egeblad, C. H. Christensen and M. Kustova, *Chem. Mater.*, 2008, **20**, 946; Y. Tao, H. Kanoh, L. Abrams and K. Kaneko, *Chem. Rev.*, 2006, **106**, 896; R. Srivastava, N. Iwasa, S. Fujita and M. Arai, *Chem.–Eur. J.*, 2008, **14**, 9507; M. Choi, H. S. Cho, R. Srivastava, C. Venkatesan, D. H. Choi and R. Ryoo, *Nat. Mater.*, 2006, **5**, 718; O. C. Gobin, S. J. Reitmeier, A. Jentys and J. A. Lercher, *J. Phys. Chem. C*, 2009, **113**, 20435.
7 L. Tosheva and V. P. Valtchev, *Chem. Mater.*, 2005, **17**, 2494; B. T. Holland, L. Abrams and A. Stein, *J. Am. Chem. Soc.*, 1999, **121**, 4308; C. J. H. Jacobsen, C. Madesen, J. Houzvicka, I. Schmidt and A. Carlsson, *J. Am. Chem. Soc.*, 2000, **122**, 7116; Y. S. Tao, H. Kanoh and K. Kaneko, *J. Am. Chem. Soc.*, 2003, **125**, 6044; M. Choi, H. S. Cho, R. Srivastava, C. Venkatesan, D. H. Choi and R. Ryoo, *Nat. Mater.*, 2006, **5**, 718; H. Wang and T. J. Pinnanvaia, *Angew. Chem., Int. Ed.*, 2006, **45**, 7603; D. P. Serrano, J. Aguado, J. M. Escola, J. M. Rodriguez and A. Peral, *Chem. Mater.*, 2006, **18**, 2462.
8 M. Choi, K. Na, J. Kim, Y. Sakamoto, T. Osamu and R. Ryoo, *Nature*, 2009, **461**, 246; K. Na, M. Choi, W. Park, Y. Sakamoto, O. Terasaki and R. Ryoo, *J. Am. Chem. Soc.*, 2010, **132**, 4169; K. Na, W. Park, Y. Seo and R. Ryoo, *Chem. Mater.*, 2011, **23**, 1273.
9 K. Na, C. Jo, J. Kim, K. Cho, J. Jung, Y. Seo, R. J. Messinger, B. F. Chmelka and R. Ryoo, *Science*, 2011, **333**, 328.
10 A. Corma, V. Fornés, S. B. Pergher, T. L. M. Maesen and J. G. Buglass, *Nature*, 1998, **396**, 353; V. V. Narkhede and H. Gies, *Chem. Mater.*, 2009, **21**, 4339.
11 A. Corma, U. Diaz, M. E. Domine and V. Fornes, *J. Am. Chem. Soc.*, 2000, **122**, 2804.
12 W. J. Roth, O. V. Shvets, M. Shamzhy, P. Chlubná, M. Kubů, P. Nachtigall and J. Čejka, *J. Am. Chem. Soc.*, 2011, **133**, 6130.
13 L. R. Aramburo, L. Karwacki, P. Cubillas, S. Asahina, D. A. M. de Winter, M. R. Drury, I. L. C. Buurmans, E. Stavitski, D. Mores, M. Daturi, P. Bazin, P. Dumas, F. Thibault-Starzyk, J. A. Post, M. W. Anderson, O. Terasaki and B. M. Weckhuysen, *Chem.–Eur. J.*, 2011, **17**, 13773.
14 J. Kim, M. Choi and R. Ryoo, *J. Catal.*, 2010, **269**, 219.

 